Time-reversal invariant topological skyrmion phases

R. Flores-Calderon and Ashley M. Cook
Max Planck Institute for the Physics of Complex Systems, Nöthnitzer Strasse 38, 01187 Dresden, Germany
and Max Planck Institute for Chemical Physics of Solids, Nöthnitzer Strasse 40, 01187 Dresden, Germany

(Received 30 June 2023; accepted 3 November 2023; published 1 December 2023)

Topological phases realized in time-reversal invariant (TRI) systems are foundational to the experimental study of the broader canon of topological condensed matter as they do not require exotic magnetic orders for realization. We therefore introduce topological skyrmion phases of matter realized in TRI systems as a foundational step towards experimental realization of topological skyrmion phases. A different bulk-boundary correspondence hidden from the tenfold way classification scheme is revealed by the presence of a nontrivial value of a $\mathbb{Z}_2$ spin skyrmion invariant. This quantized topological invariant gives a finer description of the topology in two-dimensional (2D) TRI systems as it indicates the presence or absence of robust helical edge states for open boundary conditions, in cases where the $\mathbb{Z}_2$ invariant computed with projectors onto occupied states takes a trivial value. Physically, we show that this hidden bulk-boundary correspondence derives from additional spin momentum locking of the helical edge states associated with the topological skyrmion phase.. ARPES techniques and transport measurements can detect these signatures of topological spin-momentum-locking and helical gapless modes. Our work therefore lays the foundation for experimental study of these phases of matter.

DOI: 10.1103/PhysRevB.108.235102

I. INTRODUCTION

Topological phases of matter have challenged our understanding since the discovery of the integer and fractional quantum Hall effects [1–3] and the prediction of the paradigmatic Chern insulator [4,5], culminating in the experimental realization of the quantum spin Hall insulator (QSHI) [6–14] followed by the three-dimensional (3D) topological insulator (TI) [15–21]. Due to the natural time-reversal (TR) symmetry of most experimental setups, many materials with TR-invariant topology have been identified such as in TI ultrathin films [22–24], van der Waals heterostructures [25–28], and transition-metal dichalcogenides in particular, given their large spin-orbit coupling [29,30]. These exotic states of matter present distinct bulk and edge properties generically characterized by topological invariants [31–37]. In the case of effectively noninteracting topological phases, it is well known [32,38,39] that a nontrivial topological invariant characterizes the topological phase in the bulk and implies the presence or absence of topologically robust metallic edge states which persist up to closing of the minimum direct bulk energy gap when the symmetries protecting the topological phase are respected [6,9,17–20,40]. These topological phases correspond to topologically nontrivial mappings from the full Brillouin zone (BZ) to the space of projectors onto occupied states [31,32,38,39,41], with the number of topologically distinct sectors defined by homotopy groups. An equivalent classification scheme is also derived by examining the nonlinear sigma models characterizing the topologically protected states localized at the boundary, with explicit calculation of homotopy groups facilitated by K-theory [31,41].

The set of mappings from the full Brillouin zone to the space of an observable $\mathcal{O}$ generally exhibits topological sectors if the mappings correspond to a nontrivial homotopy group, however [42,43]. The expectation value of $\mathcal{O}$ corresponding to such a nontrivial homotopy group can wind over the Brillouin zone to yield quantized, nontrivial topological charge for mappings in topological sectors; this topological charge is, in general, distinct from the topological charge due to winding of the projectors onto occupied states. A physically relevant degree of freedom that has been studied in previous works is spin [42–44], though only recent work [42,43] considers cases where the spin topological invariant is not locked in value to the projector topological invariant [44]. These topological phases associated with the spin degree of freedom specifically are known as topological skyrmion phases of matter [42], which are now understood to be lattice counterparts and first evidence of quantized transport of magnetic skyrmions, a quantum skyrmion Hall effect [45]. Notably, the quantization of topological charge computed as the winding of the ground state spin expectation value over the full BZ is guaranteed whenever the minimum magnitude of the ground state spin expectation value is finite, even when spin is not a conserved quantity [42,43].

II. MODELS

In the following, we consider tight-binding Hamiltonians which preserve time-reversal symmetry (TRS) and realize skyrmions in spin textures over the Brillouin zone. To construct such Hamiltonians, we combine a TRS-breaking

Hamiltonian, which realizes a topological skyrmion phase, with its time-reversed partner, and couple these two Hamiltonians with additional spin-orbit coupling (SOC) terms. This approach takes inspiration from construction of some Hamiltonians describing QSHI, by pairing a Chern insulator with its time-reversed partner, and then adding nonnegligible SOC terms [6,7,9]. A similar construction was used to realize first examples of helical topological skyrmion phases [42] characterized by nontrivial skyrmion numbers computed for mirror subsectors, equal in magnitude and opposite in sign. The present work goes beyond this past study in that block diagonalization is not required, and time-reversal symmetry is present. While topological skyrmion phases of matter are realized by three-band Bloch Hamiltonians [45], the simplest cases of topological skyrmion phases are, arguably, in four-band models with generalized particle-hole symmetry [42,43], therefore we consider an eight-band model. The additional degree of freedom has to be given by the spin of the electron since the four-band models possess no TR symmetry. We therefore reinterpret the skyrmion for each spin sector as forming in the texture of a pseudospin degree of freedom over the Brillouin zone. This is consistent with past work on topological skyrmion phases: ultimately, any pseudospin with the appropriate set of deformations to yield a nontrivial homotopy group has the potential to realize a topological skyrmion phase [45].

Explicitly, we consider the following Hamiltonian for the time-reversal invariant (TRI) topological skyrmion phase:

$$H_1(\mathbf{k}) = s_0[\sin k_y \tau_0 \sigma_y + \epsilon(k_x, k_y)\tau_z\sigma_z] + \sin k_x s_z \tau_z \sigma_x + \Delta(k_x, k_y) + V_{\mathrm{SOC}} + V_{\mathrm{bulk}}, \quad (1)$$

where $s_\mu, \tau_\mu, \sigma_\mu, \ \mu = 0, 1, 2, 3$ are Pauli matrices acting on the spin, particle-hole, and pseudospin degrees of freedom, respectively. We have defined $\epsilon(\mathbf{k}) = 2 + M - t(\cos k_x + \cos k_y)$, where t, M are real numbers describing hopping and staggered potential amplitudes. We further restrict ourselves to spin-triplet pairing in the pseudospin sector $\Delta(\mathbf{k}) = \Delta_0(\sin k_x s_0 \tau_y \sigma_0 - \sin k_y s_z \tau_x \sigma_z)$, where Δ_0 is the pairing strength, and spin orbit coupling term $V_{\mathrm{SOC}} = c s_x \tau_0 \sigma_y$.

Given the high symmetry of the Hamiltonians, there is some possibility of other symmetries protecting other topological phases besides those characterized by the $\mathbb{Z}_2$ projector invariant of the QSHI, or the skyrmion invariant. We therefore also include the term V_{bulk}, which may contain additional perturbations to break all symmetries save for particle-hole symmetry and time-reversal symmetry as discussed below. For negligible SOC, this Hamiltonian consists of two topological skyrmion phase Hamiltonians, which possess a total Chern number $\mathcal{C}_{\mathrm{tot}}$ of $+2$ or -2 and skyrmion number $\mathcal{Q}$ of -1 or $+1$ for half-filling, respectively, depending on the spin sector. For nonnegligible SOC, this corresponds to a trivial value for the $\mathbb{Z}_2$ projector topological invariant of the quantum spin Hall insulator phase, and a nontrivial value for the $\mathbb{Z}_2$ skyrmion topological invariant.

To explore the consequences of the nontrivial skyrmion topology, we additionally consider a counterpart TRS Hamiltonian constructed from topological skyrmion phase Hamiltonians with an even total Chern number and even skyrmion number:

$$H_2(\mathbf{k}) = s_0[t\cos k_x \tau_z \sigma_x + \cos(k_x + k_y)\tau_z\sigma_z] + t\cos k_y s_z \tau_0 \sigma_y + \Delta(k_x, k_y) + V_{\mathrm{SOC}}. \quad (2)$$

As these two Hamiltonians each possess particle-hole symmetry (PHS), they can be written in the Nambu basis to describe superconductors at mean-field level using Bogoliubov de Gennes formalism [46,47]. Equations (1) and (2) are invariant under the particle-hole operators $\mathcal{C}_1 = s_z\tau_x\sigma_z K$ and $\mathcal{C}_2 = \tau_x K$, respectively, which each square to one. By construction, each model is also invariant under the spinful time-reversal operation $\mathcal{T} = -is_y K$.

III. TOPOLOGICAL CHARACTERIZATION

To characterize the topology of these models, we employ a generalization of the skyrmion invariant to TRI systems. The use of the total skyrmion number to characterize the topology fails since, in analogy to the Chern number, it is always zero when spinful TRS is present, as proved in Appendix S1 [48]. In the case of the quintessential two-dimensional (2D) TR-invariant systems classified by the tenfold way, one can construct a nonzero topological invariant in multiple equivalent formalisms. One such path involves the usage of Kramer's theorem to express the Hamiltonian in terms of the helicity basis or Kramers pair basis, where the Hamiltonian is block diagonal. This can be done in the case of negligible SOC. Then, for each Hamiltonian one can calculate the Chern number and define a parity index $\nu = (C - C_{TR})/2 \ \mathrm{mod}(2) = (-1)^C$. The parity index is equivalent to the celebrated $\mathbb{Z}_2$ invariant of Kane-Mele [6,9].

In analogy to this parity invariant, we may compute a skyrmion number for each spin sector, characterizing a topological pseudospin texture over the Brillouin zone. The explicit form of the spin operators is given in Appendix S2 [48] and a schematic visualization of this mapping is shown in Fig. 1. Once these operators are defined, the topological skyrmion invariant can be calculated for each spin sector so as to obtain two $\mathcal{Q}_I, \mathcal{Q}_{II} \in \mathbb{Z}$ integers. As detailed in Appendix S2 [48], these quantities are opposite in sign and equal in magnitude so that it is natural to define a *TR-skyrmion invariant* or *skyrmion parity* given by $\nu_{\mathcal{Q}} = (\mathcal{Q}_I - \mathcal{Q}_{II})/2 \ \mathrm{mod}(2)$. This invariant, which now fully takes into account the TR-invariant nature of the system, will be shown to be linked to a bulk-boundary correspondence when open boundary conditions (OBC) in x or y are applied. It will be further shown numerically that the helical edge states that present when the TR-skyrmion invariant is nontrivial are robust to disorder and local perturbations. Furthermore, the remarkable behavior displayed by this phase does not rely on crystalline point group symmetries, as will be shown by explicitly breaking all symmetries except for time reversal and particle hole.

IV. RESULTS

Starting with the simplest case of negligible spin-orbit coupling, we consider two uncoupled Hamiltonians labeled by spin sector, which each possess four bands, with a well-defined Chern number and skyrmion number as described

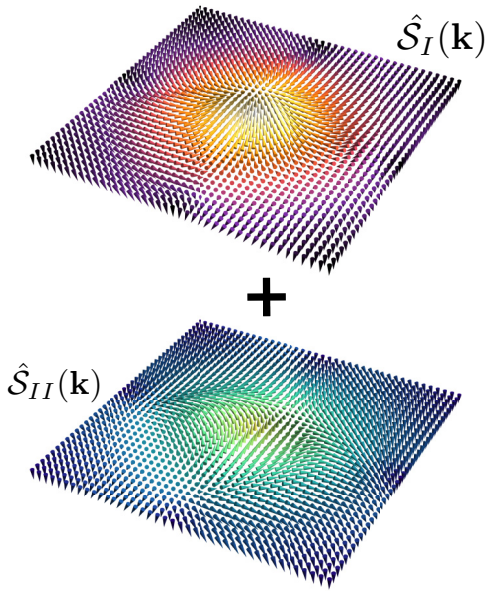

FIG. 1. Pseudospin textures of the TR skyrmion phase analyzed in the main text. The arrows represent the pseudospin expectation value $\langle S^I_\mu \rangle_{\mathbf{k}}$ for one TR sector denoted by I, and this skyrmion texture has a TR partner (lower skyrmion texture), which is given by the pseudospin expectation value $\langle S^{II}_\mu \rangle_{\mathbf{k}}$ of the II TR sector. The color is proportional to the polar angle of the texture. The skyrmion numbers correspond to $\mathcal{Q}_I = +1$, $\mathcal{Q}_{II} = -1$ for the model of (1) with $M = -1$, $\Delta_0 = 0.5$, $\lambda = 0.3$, and $c = 0.5$.

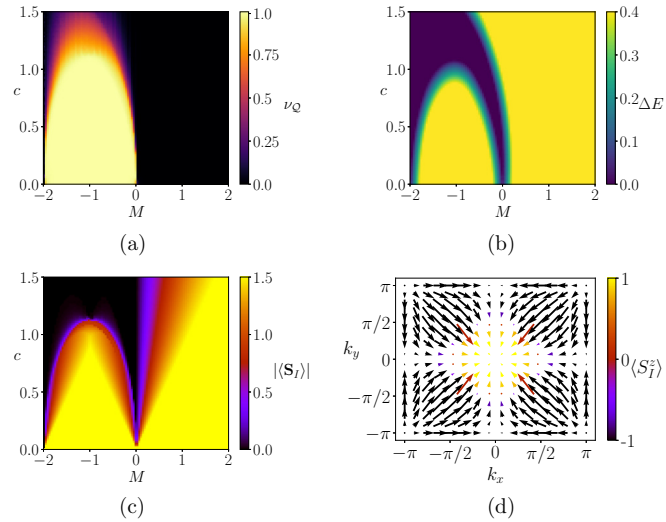

FIG. 2. (a) Phase diagram of the TR-skyrmion invariant $\nu_{\mathcal{Q}}$ for a fixed value of $\Delta_0 = 0.5$ and bulk perturbation $\lambda = 0.3$ of model (1). (b) Minimum direct gap as a function of c and M for the same parameter values. (c) Minimum pseudospin magnitude for the first TR or spin up sector. (d) Skyrmion texture for vanishing magnitude $c = 1.5$, $M = -1$, for the first TR sector, the arrows represent the vector $(\langle S^x_I \rangle, \langle S^y_I \rangle)$ while the color represents $\langle S^z_I \rangle$.

in Liu *et al.* [43]. For $H_1(\mathbf{k})$ the total Chern number of each sector takes only two nontrivial values $C_I = \pm 2$ and $C_{II} = -C_I$ because of TRS. As the topological invariant for a quantum spin Hall insulator with nonnegligible SOC according to the tenfold way classification scheme is $\nu = (C_I - C_{II})/2 \ \mathrm{mod}(2)$, the value of ν for our Hamiltonian is then always trivial as $\nu = 2 \ \mathrm{mod}(2) = 0 \ \mathrm{mod}\ 2$.

In contrast, $\mathcal{Q}_I = \mp 1$ in the regions of the phase diagram where $C_I = \pm 2$. Therefore, the skyrmion number for the TRI system $\nu_{\mathcal{Q}}$ evaluates to $\nu_{\mathcal{Q}} = (\mathcal{Q}_I - \mathcal{Q}_{II})/2 \ \mathrm{mod}(2) = 1 \ \mathrm{mod}(2)$ for these regions of the phase diagram. The system with nonnegligible SOC is therefore in a topologically nontrivial phase according to the skyrmion invariant, even when the projector invariant indicates the system is topologically trivial.

To explore the consequences of the nontrivial skyrmion number paired with the trivial projector topological invariant, we consider the case of the trivial projector invariant and trivial skyrmion number by comparing results for the Hamiltonian given by Eq. (1) with those for the Hamiltonian given by Eq. (2). In the case of Eq. (2), $C_I = \pm 4$ in the topologically nontrivial regions of the phase diagram, corresponding to $\nu = 0$ when SOC is nonnegligible, and $\mathcal{Q}_I = \mp 2$, yielding a trivial $\nu_{\mathcal{Q}} = 0$ as well. Comparing these two cases, we observe additional structure that is captured by the skyrmion invariant, which is richer than the tenfold way classification scheme.

The previous analysis is valid when no SOC term is present. For ν even, it is known that as long as V_{SOC} does not break TRS and does not close the minimum direct bulk energy gap, then the invariant will always be trivial and the system is expected to be topologically trivial. We therefore explore the effects of nonnegligible SOC in systems characterized by the ν invariant, but also the previously unidentified skyrmion invariant $\nu_{\mathcal{Q}}$.

Having defined this TR-skyrmion invariant $\nu_{\mathcal{Q}}$, we compute phase diagrams characterizing the skyrmion topology for Hamiltonian Eq. (1), which are shown in Fig. 2. $\nu_{\mathcal{Q}}$ is shown in Fig. 2(a) for $\Delta_0 = 0.5$, as a function of SOC constant c and mass parameter M. To understand the stability of the TRI topological skyrmion phase and corresponding quantization of $\nu_{\mathcal{Q}}$, we also show the minimum direct bulk energy gap ΔE in Fig. 2(b) and the minimum spin magnitude $|\langle S_I \rangle|$ in Fig. 2(c), respectively, each as a function of c and M. For this parameter set, two regimes are distinguished in the case of $H_1(\mathbf{k})$: the trivial regime of zero skyrmion number, and the region of $\mathcal{Q}_I = \pm 1$, $\mathcal{Q}_{II} = \mp 1$. Quantization of $\nu_{\mathcal{Q}}$ survives for finite c and is nontrivial for the regime $-2 < M < 0$ when each of ΔE and $|\langle S_I \rangle|$ are finite. For sufficiently large c, $|\langle S_I \rangle|$ goes to zero, and $\nu_{\mathcal{Q}}$ is finite but unquantized, smoothly approaching zero with further increase of c. The pseudospin texture corresponding to one of these unquantized values of $\nu_{\mathcal{Q}}$ is shown in Fig. 2(d). This situation is analogous to the loss of quantization of the Hall conductivity in a Chern insulator when the Fermi level intersects bands, rather than bands being completely filled or empty.

For this model, $\nu_{\mathcal{Q}}$ only changes when $\Delta E = 0$ corresponding to a type-I topological phase transition. This corresponds to symmetry protection of two sets of spin operators, each with 4×4 matrix representation, as opposed to a lower-symmetry model with a single set of spin operators with 8×8 matrix representations: we have effectively two four-band toy models for topological skyrmion phases still despite finite SOC terms, and it is previously known

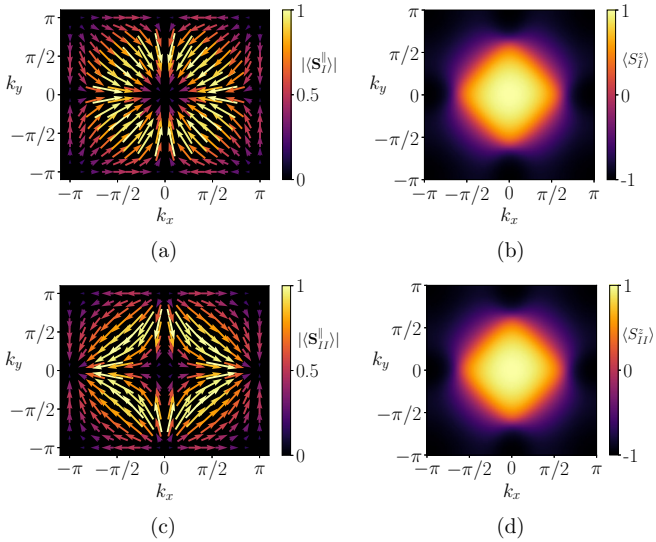

FIG. 3. Normalized ground state pseudospin expectation value plots for the model of (1) with $M = -1.3$, $\Delta_0 = 0.5$, $\lambda = 0.4$, and $c = 0.8$. (a) and (c) show the x-y pseudospin texture and normalized $|\langle[\mathcal{S}_x^I(\mathbf{k}), \mathcal{S}_y^I(\mathbf{k})]\rangle|$, $|\langle[\mathcal{S}_x^{II}(\mathbf{k}), \mathcal{S}_y^{II}(\mathbf{k})]\rangle|$, respectively. (b) and (d) show the normalized z component of the pseudospin texture $\langle \mathbf{S}_I^z\rangle$ and $\langle \mathbf{S}_{II}^z\rangle$, respectively.

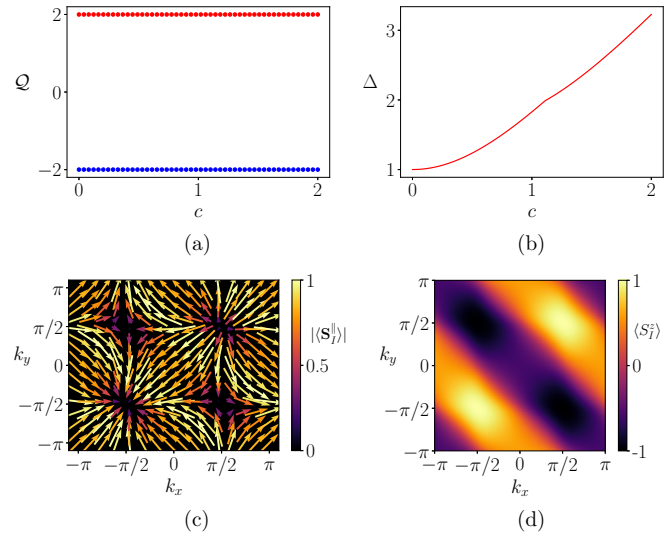

FIG. 4. (a) Skyrmion numbers $\mathcal{Q}_I$ (red) and $\mathcal{Q}_{II}$ (blue) computed for $M = 1$, $\Delta_0 = 0.5$ as a function of SOC c for the model Hamiltonian of Eq. (2). (b) Minimum direct gap between bands enclosing zero Fermi energy. (c and d) Normalized ground state pseudospin expectation value plots with $t = 1$, $\Delta_0 = 0.5$, $\lambda = 0.4$, and $c = 0.5$. (c) shows the x-y pseudospin texture $|\langle[\mathcal{S}_x^I(\mathbf{k}), \mathcal{S}_y^I(\mathbf{k})]\rangle|$, while (d) shows the normalized z component of the pseudospin texture $\langle \mathbf{S}_I^z\rangle$.

that four-band models for topological skyrmion phases with generalized particle-hole symmetry $\mathcal{C}'$ lack sufficient degrees of freedom to realize the type-II topological phase transition [43], although three-band models without $\mathcal{C}'$ symmetry realize type-II topological phase transitions quite generically [45].

An example of the skyrmion texture with $\mathcal{Q}_I = +1$, with $M = -1.3$, $\Delta_0 = 0.5$, and $c = 0.8$ is shown in Figs. 3(a) and 3(b). The time reverse partner with the antiskyrmion $\mathcal{Q}_{II} = -1$ is shown in Figs. 3(c) and 3(d) for the same parameter values.

We now include the effect of a symmetry-breaking term additionally to the normal SOC given by

$$V_{\text{bulk}}(\mathbf{k}) = \lambda[\sin(k_x + k_y)\cos(k_y)s_y\tau_x\sigma_0 + \sin(k_x)s_x\tau_z\sigma_0]. \tag{3}$$

This extra term in the Hamiltonian breaks all spurious crystalline symmetries of the original Hamiltonian in Eq. (1). Included in those symmetries is inversion so that inversion is broken in the bulk as well as $\mathcal{C}'$ symmetry. The only remaining symmetries in the model are particle-hole $\mathcal{C}$ and time-reversal $\mathcal{T}$ symmetry as well as the combined chiral $\mathcal{CT}$.

Figure 3 shows a winding within each of the two TR sectors (I and II) that remains even with nonnegligible SOC.

An important region of the phase diagram is the zero energy and zero pseudospin magnitude regime above approximately $c = 1.2$. In this case, because of the gapless spectrum, the skyrmion number destabilizes and $\mathcal{Q}_I$, $\mathcal{Q}_{II}$ are not well defined just as the prototypical $\mathbb{Z}_2$ invariant. Remarkably, as shown in Fig. 2(d), the pseudospin still winds in such a manner that almost everywhere in the BZ it forms a skyrmion. The points of zero spin magnitude seem to not deform the global structure that give rise to the skyrmion texture, although the TR skyrmion invariant is destabilized in this case.

It is worth noting that we can also do the same analysis for the second Hamiltonian $H_2(\mathbf{k})$; in this case the pseudospin textures for each TR subsector result in a quantized skyrmion invariant of ± 2 and thus not only a trivial projector invariant but also a trivial skyrmion parity. This is shown as a function of SOC in Fig. 4 along with an example of a skyrmion texture. It is worth mentioning that even if the skyrmion parity is trivial across the phase diagram, we still observe quantization of the skyrmion invariant as well as the nontrivial relation $Q_I = -Q_{II}$ holding for all parameter values.

V. BULK-BOUNDARY CORRESPONDENCE

The two Hamiltonians, Eqs. (1) and (2), each possess a $\mathcal{C}'$-invariant Chern insulator with even Chern number and its TR partner. For Eq. (1), the magnitude of this Chern number is 2, and for Eq. (2), it is 4. For nonnegligible SOC or other perturbations breaking S_z conservation, the $\mathbb{Z}_2$ projector invariant calculated from $\nu = (C - C_{TR})/2 \bmod(2)$ will always be trivial for these even Chern numbers as long as the bulk gap does not close according to the tenfold way [32,39]. One therefore expects the edge states present for zero SOC associated with the Chern insulators will hybridize and gap out immediately for finite coupling between the sectors related by TRS. More generally, all even Chern number Hamiltonians coupled to their TR partners are predicted to yield a topologically trivial phase due to $\mathbb{Z}_2$ classification in these cases.

We observe a counterexample to this statement, that all Hamiltonians with an even total Chern number coupled to their TR partners are predicted to yield a topologically trivial phase, for ν_Q odd in value, however. We first consider the Hamiltonians Eqs. (1) and (2) for $\lambda = 0$, $c = 0$

corresponding to negligible SOC and negligible bulk perturbation, respectively. Each exhibits localized edge states in its slab spectrum that connect bulk conduction and valence bands. We observe an even number of Kramers pairs at the boundary, in agreement with TR symmetry. For a QSHI, finite c corresponding to the nonnegligible SOC term is expected to gap out the helical edge modes as the topological classification associated with mappings to projectors onto occupied sites reduces from $\mathbb{Z}$ to $\mathbb{Z}_2$. However, in the model considered here, the boundary states appearing from applying OBC to the Hamiltonian (1) do not gap out for finite c and nonnegligible SOC. The helical modes instead remain gapless and localized on the edges. Furthermore, the edge states of Eq. (2) gap out for finite c corresponding to nonnegligible SOC, with the energy gap being proportional to c, as expected for a trivial phase. This shows there is some correspondence between additional robustness of the helical edge modes and ν_Q odd in value.

We further investigate the mechanism for this unexpected robustness of the helical edge modes for trivial $\mathbb{Z}_2$ projector invariant and nontrivial $\mathbb{Z}_2$ skyrmion invariant by considering λ finite, where λ is the free parameter of a bulk perturbation that breaks all symmetries of Eq. (1), except for TR and particle-hole. The results of this perturbation are summarized in Fig. 5. Figures 5(a) and 5(b) show that, even with all crystalline symmetries broken, the gapless edge states are present. This shows that the gapless edge states are not protected by crystalline point group symmetries of the bulk.

We investigate the robustness of the gapless modes against edge perturbations. Figures 5(c) and 5(d) show the slab spectra for an additional edge perturbation in Eq. (1), which has previously been shown to gap edge states of the QSHI [49]:

$$V_{\text{edge}}(y, k_x) = \begin{cases} V_1 \cos(k_x) s_0 \tau_0 \sigma_z & y = 0 \\ -V_1 \sin(k_x) s_x \tau_z \sigma_0 & y = N_y \\ 0 & \text{else.} \end{cases} \tag{4}$$

This perturbation can also be applied for the case of OBC in the x direction by interchanging the x and y labels in its definition. As is clear from the plots in Figs. 5(a)–5(d), the gapless points may shift, but they remain present even in the presence of spin-orbit coupling.

We also investigate the effects of on-site disorder on the edge dispersion and localization of the edge states protected by the skyrmion topology. We add on-site disorder of the form $V_j s_0 \tau_z \sigma_0$ for OBC in y, with j being the layer index. This form of disorder preserves time-reversal and particle-hole symmetries. The effects on the energy spectrum are shown in Figs. 5(e) and 5(f), respectively. We find that the gapless edge states persist in the presence of a random disorder realization, as shown in Fig. 5(e). To compute corresponding disorder-averaged results, we compute the spectrum of Eq. (1) in this slab geometry for each k_x, and then combine these energy eigenvalues for each k_x into a single larger array, which we then sort in energy. This is computed for each of 100 disorder realizations, and the average of these sorted spectra is shown in Fig. 5(f). We find the edge states of this disorder-averaged spectrum remain gapless, corresponding to each disorder realization simply shifting the crossing point of the helical modes in k_x.

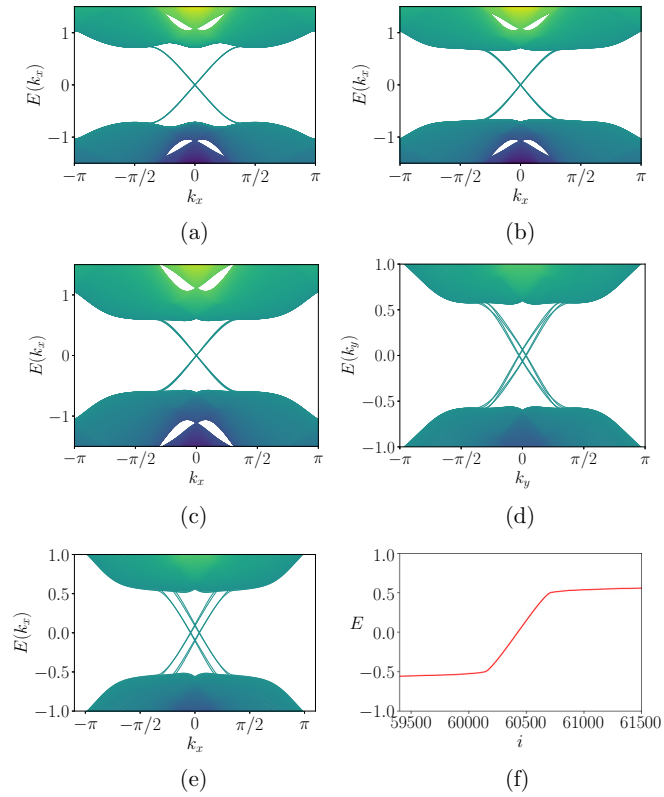

FIG. 5. (a) Energy spectrum for the model of Eq. (1) with OBC in y and periodic in x with parameters $M = -1$, $\Delta_0 = 0.5$, $c = 0.4$, length $N_y = 200$, and $\lambda = 0.0$. (b) Energy spectrum for the same conditions except $\lambda = 0.3$. (c) Edge spectrum with OBC in y for $M = -1$, $\Delta_0 = 0.5$, $c = 0.5$, and $\lambda = 0.3$ with the edge perturbation discussed in the text $V_1 = 0.1$. (d) Same parameters and perturbation but now with OBC in x. (e) Edge spectrum with OBC in y for the same parameters as (c) but with some random disorder realization respecting particle-hole and TR. (d) Same parameters and perturbation but now with OBC in x. (f) Energy spectrum as a function of eigenvalue index i for a disorder average over 100 on-site potentials $V_j s_0 \tau_z \sigma_0$ distributed with zero mean and standard deviation 0.1. For a system with open boundary conditions in y, periodic in x and parameters $M = -1$, $\Delta_0 = 0.5$, $c = 0.5$, and $\lambda = 0.3$.

We now also explore how the nontrivial skyrmion invariant ν_Q alters the character of the edge states to prevent hybridization. Given related work introducing the observable-enriched partial trace and characterizing the additional spin momentum locking of edge states due to nontrivial skyrmion number, we compute the pseudospin expectation values for the edge states for a given TR sector in a slab geometry with either x or y directions open so as to have k_y or k_x as a good quantum number. We find that, even though nonneglible SOC is present, the edge state pseudospin texture has a very distinct pattern depending on the orientation of the edge. For open boundary conditions in the y direction, near the crossing of the edge modes the pseudospin $\langle S_y^I \rangle$, $\langle S_z^I \rangle$ seems to average to zero for each edge, while $\langle S_x^I \rangle$ does not, as seen in Fig. 6. Instead the value of $\langle S_x^I \rangle$ on each edge seems to be minus the one of the other edge.

We additionally confirm the nontrivial nature of the edge states by computing the σ_{xx} conductivity as a function of

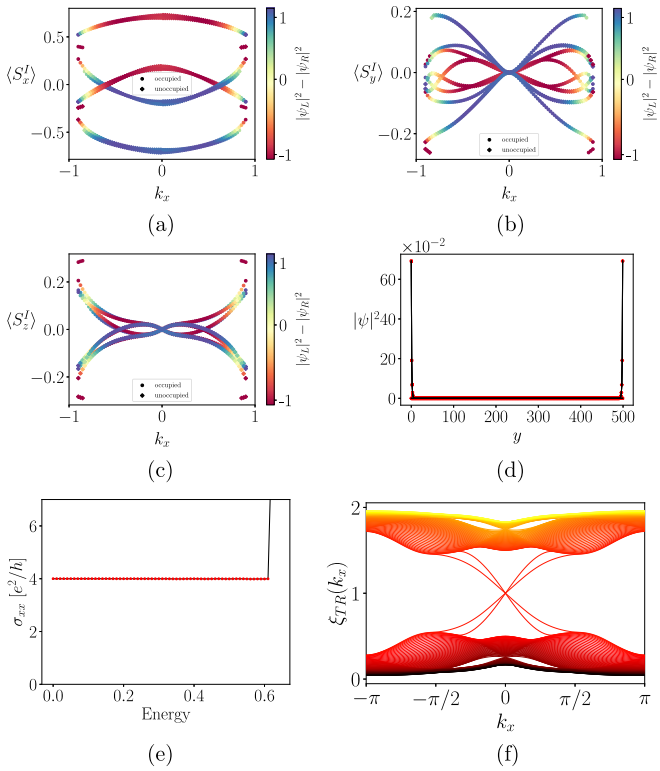

FIG. 6. (a) x component of the pseudospin expectation value for the edge states of the Hamiltonian in Eq. (1) with parameters $M = -1$, $\Delta_0 = 0.5$, $\lambda = 0.3$, $c = 0.5$ and open boundary conditions on y. The color is proportional to the localization on either edge, computed by taking the probability density at each edge and subtracting them. (b) and (c) show the y, z components of the pseudospin expectation value for the edge states, respectively. (d) Probability density for the edge states of the Hamiltonian in Eq. (1). (e) Conductivity along xx as a function of energy for the Hamiltonian in Eq. 1 with parameters $M = -1$, $\Delta_0 = 0.5$, $\lambda = 0.0$, $c = 0.5$ and full open boundary conditions; random Gaussian disorder along the whole sample with standard deviation 0.01 is present. (f) Two-point reduced correlation spectrum for the Hamiltonian in Eq. 1 with parameters $M = -1$, $\Delta_0 = 0.5$, $\lambda = 0.3$, $c = 0.5$ and all $\mathcal{T}, \mathcal{C}$ symmetry allowed perturbations with amplitude 0.5 turned on, for a cut along the y axis and traced over $L = 200$ lattice sites and particle-hole degree of freedom.

energy as shown in Fig. 6(e). Here, the conduction band of the system starts around 0.6 in units of the hopping, since this was set to be one by default, and so a trivial zero conductance would be expected below it. Instead a quantized longitudinal conductivity of $4e^2/h$ appears, even in the presence of disorder. Such a signature implies the existence of transmission channels present in the system which necessarily come from edge state transmission since the bulk material is an insulator [50–52]. Specifically for the case of the QSHI, it has been shown that a quantized transport robust to disorder, as in Fig. 6(e), is indeed linked to the presence of topologically protected edge states which for the QSHI carry a $2e^2/h$ conductance [53]. We indeed observe a quantization to $4e^2/h$ consistent with the four edge states per edge which appear when opening boundary conditions as discussed in the previous paragraphs. The robustness to disorder for this $\nu = 0$, $\nu_{\mathcal{Q}} = 1$ case is consistent with quenching of SOC by the topological spin polarization of the edge states that is part of the bulk-boundary correspondence of topological skyrmion phases of matter. We may also understand it from the perspective of the lower-symmetry realizations of topological skyrmion phases in the study of the quantum skyrmion Hall effect [45]: three-band tight-binding models for topological skyrmion phases of matter without $\mathcal{C}'$ symmetry realize generalized Thouless pumps, in which spin angular momentum is pumped, rather than electric charge. The spin polarization of edge states observed here corresponds to a $\mathcal{C}'$-symmetric and TR-symmetric Thouless pump of spin angular momentum, and gaplessness of edge states is required for this pumping in correspondence with nontrivial ν_Q.

However, the most robust astonishing feature associated with the skyrmion invariant is seen upon tracing out the particle-hole degree of freedom in each spin sector, by performing the observable-enriched partial trace defined in Appendix S3. That is, we characterize the skyrmion topology by tracing out the particle-hole degree of freedom—in addition to a virtual cut in real space [54]—to compute a reduced two-point function and corresponding entanglement spectrum computed from the ground state as seen in Fig. 6(f). In correspondence with the nontrivial skyrmion invariant, this observable-enriched entanglement spectrum exhibits helical edge modes. We may therefore understand the spin polarization of edge states in the full system as consequences of the bulk-boundary correspondence of a potentially open subsystem, realized by tracing out the particle-hole degree of freedom.

In addition to the previous characterization of the edge states, we finally also explore the remarkable robustness of the gapless helical edge modes for trivial projector invariant and nontrivial skyrmion invariant, by enumerating all possible spin-orbit coupling terms that preserve time-reversal symmetry and particle-hole symmetry. Out of all possible six momentum-even terms, the gapless helical edge modes are robust against three of these terms, and the other three gap them out. These terms are provided in Appendix S4 [48]. We distinguish the three SOC terms, preserving the gapless helical edge modes from those which gap them out by additional symmetry protection.

First, we find that certain 4×4 submatrices of the Hamiltonian must preserve $(\mathcal{CT})_p$ symmetry (defined in Appendix S4 [48]), otherwise an effective Rashba SOC term is introduced, permitting finite y component of spin in sector I/II for the edge states in the vicinity of the gapless point(s) in the edge spectrum. That is, the spin momentum locking of the edge states is relaxed. As discussed in Appendix S4 [48], clockwise spin rotation about the z axis within sector I/II for one state at the edge is compensated by counterclockwise rotation of the second state at that edge within the same sector (the $\mathcal{C}'$ partner of the first state), such that the net spin of these edge states in combination remains polarized in the x direction. We may compute the observable-enriched entanglement spectrum as defined in Appendix S3 [48] to examine bulk-boundary correspondence in our system upon tracing out the particle-hole degree of freedom of each spin sector to further characterize this edge state spin texture, shown in Appendix S4 [48]. We find the spin textures are consistent with gapless states of the spin subsystem propagating along the

edge deep within the bulk gap of the entanglement spectrum. Indeed, we examine the edge spectrum of the spin subsystem explicitly to show the nontrivial spin topology is preserved in this lower-symmetry case, but the observable-enriched entanglement spectrum exhibits additional k_x-dependent Rashba splitting. This finite y spin component permits hybridization between edge states previously forced to zero by the stricter spin momentum locking for $(\mathcal{CT})_p$ preserved, gapping out the helical edge states protected by the spin topology.

Second, in this system, we have three twofold degrees of freedom, corresponding to the s, τ, and σ Pauli matrices, respectively. The symmetry operator $\mathcal{C}'$, which acts on the τ and σ degrees of freedom only (acting simply as a constant in the s sector), is required to define two skyrmion numbers, $\mathcal{Q}_I$ and $\mathcal{Q}_{II}$, computed as winding of spin $\mathcal{S}_I$ and $\mathcal{S}_{II}$ in terms of the matrices discussed in Appendix S2 [48], respectively. The precise statements of these symmetry requirements are provided in Appendix S4 [48]. This additional symmetry protection reflects the fact that the helical edge modes are being protected by topology of subsets of the degrees of freedom, and indicates that the concept of symmetry protection for topological phases must be generalized in light of the topological skyrmion phases of matter.

VI. CONCLUSIONS

In this paper, we introduce TRI topological skyrmion phases of matter. These are topological phases realized in systems with time-reversal symmetry as required to protect the quantum spin Hall insulator (QSHI) phase, but which are distinct from the QSHI phase. The QSHI is a topological phase of the tenfold way classification scheme [32], resulting from mappings from the full Brillouin zone to the space of projectors onto occupied states, while the TRI skyrmion phase arises from topologically nontrivial mappings from the full Brillouin zone to the space of ground state spin expectation values. The TRI skyrmion phases are therefore characterized in the bulk by formation of a skyrmion in the texture of the ground-state spin expectation value over the Brillouin zone in general, rather than in the texture of the projector onto occupied states over the Brillouin zone.

We construct toy models for the TRI skyrmion phase by combining the Bloch Hamiltonian invariant under generalized particle-hole conjugation $\mathcal{C}'$ but time-reversal symmetry-breaking topological skyrmion phase with its time-reversed partner into a Bloch Hamiltonian matrix representation with time-reversal symmetry. We may therefore characterize the time-reversal symmetric (TRS) skyrmion phase with two skyrmion numbers related to one another by time-reversal symmetry in simpler cases corresponding to a helical topological skyrmion phase. More generally, we may also include a spin-orbit coupling term V_{SOC} coupling these two sectors, in which case the phase is characterized by a single topological invariant $\nu_{\mathcal{Q}}$, which is equal to the skyrmion number for one sector, modulo 2. This corresponds to a more general $\mathbb{Z}_2$ classification of $\nu_{\mathcal{Q}}$.

Performing an observable-enriched partial trace on the density matrix of the occupied states for a system with open boundary conditions corresponding to a slab geometry to compute the observable-enriched reduced density matrix of the spin subsystem, we find odd $\nu_{\mathcal{Q}}$ corresponds to topologically protected gapless modes in the observable-enriched entanglement spectrum. We show this bulk-boundary correspondence of the spin subsystem has consequences for the bulk-boundary correspondence of the full system, demanding robust helical gapless edge states at the boundary of the system for open boundary conditions, even when the system is not in a quantum spin Hall insulator phase according to the $\mathbb{Z}_2$ projector invariant ν. That is, for ν even and trivial, but $\nu_{\mathcal{Q}}$ odd and nontrivial, we find topologically robust, helical gapless edge modes protected by nontrivial $\nu_{\mathcal{Q}}$. When each of ν and $\nu_{\mathcal{Q}}$ is even, topologically protected helical edge modes are absent.

We find the persistence of the helical modes for nontrivial $\nu_{\mathcal{Q}}$—when ν is trivial—is related to the strict spin momentum locking enforced on edge states in the full system by nontrivial $\nu_{\mathcal{Q}}$. This spin momentum locking derives from the requirement of gapless helical boundary modes in the observable-enriched slab entanglement spectrum of the spin subsystem due to nontrivial $\nu_{\mathcal{Q}}$ in the bulk. We add terms to the bulk Hamiltonian such that projectors onto the occupied states possess only time-reversal symmetry $\mathcal{T}$ and particle-hole symmetry $\mathcal{C}$. We find that the helical gapless modes observed for trivial ν and nontrivial $\nu_{\mathcal{Q}}$ are robust for nonnegligible spin-orbit coupling term V_{SOC} respecting a generalized particle-hole symmetry $\mathcal{C}'$ of a subset of the degrees of freedom, as well as lacking a generalized Rashba spin-orbit coupling, which softens spin momentum locking at the edge while still yielding the gapless helical edge modes of the spin subsystem after observable-enriched partial trace.

Recent work [45] demonstrates that time-reversal symmetry-breaking (TRB) topological skyrmion phases are realized in three-band Bloch Hamiltonians without particle-hole symmetry, which demonstrates that particle-hole symmetry is not required to stabilize topological skyrmion phases of matter. The role of particle-hole symmetry in the present work is only to yield a particularly simple spin representation and realize topological skyrmion phases in toy models of a particularly simple form [42,43,45]. For time-reversal-invariant topological skyrmion phases, similarly, only time-reversal symmetry is required for stabilization, and particle-hole symmetry simply yields a particular spin representation useful for studying this physics in a particular class of simple Hamiltonians. Given this, future work will include characterization of TRI topological skyrmion phases realized in time-reversal-invariant six-band models constructed from the TRB three-band models, following the construction methods presented in this work.

We expect time-reversal-invariant topological skyrmion phases realized in normal state models (without particle-hole symmetry) will exhibit more robust helical edge modes than those observed here, as well as type-II topological phase transitions [42,45]. While previous work on normal state topological skyrmion phases considers a basis and spin representation relevant to transition metal compounds [42,45], the TRI skyrmion phases are more broadly expected in normal state systems, in particular those with nonnegligible coupling of at least two degrees of freedom, such as spin and orbital, or even pseudospins such as valley or layer, including

van der Waals heterostructures or transition-metal dichalcogenides [25–28].

Notably, these helical gapless modes affect computation of the projector topological invariant: spectral flow [55] winds nontrivially in correspondence with the presence of helical gapless modes, contradicting $\mathbb{Z}_2$ classification of ν. This indicates the projector invariant ν must be generalized to incorporate changes due to $\nu_{\mathcal{Q}}$, rather than treated as independent of $\nu_{\mathcal{Q}}$. This is also consistent with results of three-band models for topological skyrmion phases, where the nontrivial total Chern number as determined by bulk spectral flow does not necessarily yield chiral transport on the edge. These failures relate to reliance of much topological characterization on the flat-band limit assumption and topological stability up to closing of a charge gap, which does not hold in general [42,45].

Topologically protected gapless helical modes and additional spin momentum locking may then be observed in transport measurements or spin-ARPES and serve as important signatures and consequences of topological skyrmion phases of matter. The realization of these signatures in time-reversal invariant systems is also highly desirable for experiment, as the nontrivial topology is realized without the need for particular magnetic orders which generally complicate experimental realization. Our work is therefore significant in bringing the study of topological skyrmion phases—including their role in extending topological classification schemes—much closer to experimental realization.

ACKNOWLEDGMENTS

The authors are grateful to R. Ay and J. H. Winter for helpful discussions. This research was supported in part by the National Science Foundation under Grants No. NSF PHY-1748958 and No. PHY-2309135, and undertaken in part at Aspen Center for Physics, which is supported by National Science Foundation Grant No. PHY-2210452.

[1] K. v. Klitzing, G. Dorda, and M. Pepper, New method for high-accuracy determination of the fine-structure constant based on quantized Hall resistance, Phys. Rev. Lett. **45**, 494 (1980).

[2] D. C. Tsui, H. L. Stormer, and A. C. Gossard, Two-dimensional magnetotransport in the extreme quantum limit, Phys. Rev. Lett. **48**, 1559 (1982).

[3] R. B. Laughlin, Anomalous quantum Hall effect: An incompressible quantum fluid with fractionally charged excitations, Phys. Rev. Lett. **50**, 1395 (1983).

[4] C.-Z. Chang, J. Zhang, X. Feng, J. Shen, Z. Zhang, M. Guo, K. Li, Y. Ou, P. Wei, L.-L. Wang, Z.-Q. Ji, Y. Feng, S. Ji, X. Chen, J. Jia, X. Dai, Z. Fang, S.-C. Zhang, K. He, Y. Wang *et al.*, Experimental observation of the quantum anomalous Hall effect in a magnetic topological insulator, Science **340**, 167 (2013).

[5] F. D. M. Haldane, Model for a quantum Hall effect without Landau levels: Condensed-matter realization of the "parity anomaly," Phys. Rev. Lett. **61**, 2015 (1988).

[6] C. L. Kane and E. J. Mele, Quantum spin Hall effect in graphene, Phys. Rev. Lett. **95**, 226801 (2005).

[7] B. A. Bernevig, T. L. Hughes, and S.-C. Zhang, Quantum spin Hall effect and topological phase transition in HgTe quantum wells, Science **314**, 1757 (2006).

[8] M. König, S. Wiedmann, C. Brüne, A. Roth, H. Buhmann, L. W. Molenkamp, X.-L. Qi, and S.-C. Zhang, Quantum spin Hall insulator state in HgTe quantum wells, Science **318**, 766 (2007).

[9] C. L. Kane and E. J. Mele, Z_2 topological order and the quantum spin Hall effect, Phys. Rev. Lett. **95**, 146802 (2005).

[10] Y. Yao, F. Ye, X.-L. Qi, S.-C. Zhang, and Z. Fang, Spin-orbit gap of graphene: First-principles calculations, Phys. Rev. B **75**, 041401(R) (2007).

[11] B. Zhou, H.-Z. Lu, R.-L. Chu, S.-Q. Shen, and Q. Niu, Finite size effects on helical edge states in a quantum spin-Hall system, Phys. Rev. Lett. **101**, 246807 (2008).

[12] L. Ulčakar, J. Mravlje, A. Ramšak, and T. Rejec, Slow quenches in two-dimensional time-reversal symmetric $\mathbb{Z}_2$ topological insulators, Phys. Rev. B **97**, 195127 (2018).

[13] H. Min, J. E. Hill, N. A. Sinitsyn, B. R. Sahu, L. Kleinman, and A. H. MacDonald, Intrinsic and Rashba spin-orbit interactions in graphene sheets, Phys. Rev. B **74**, 165310 (2006).

[14] X. Qian, J. Liu, L. Fu, and J. Li, Quantum spin Hall effect in two-dimensional transition metal dichalcogenides, Science **346**, 1344 (2014).

[15] L. Fu, C. L. Kane, and E. J. Mele, Topological insulators in three dimensions, Phys. Rev. Lett. **98**, 106803 (2007).

[16] D. Hsieh, Y. Xia, L. Wray, D. Qian, A. Pal, J. H. Dil, J. Osterwalder, F. Meier, G. Bihlmayer, C. L. Kane, Y. S. Hor, R. J. Cava, and M. Z. Hasan, Observation of unconventional quantum spin textures in topological insulators, Science **323**, 919 (2009).

[17] J. Noh, W. A. Benalcazar, S. Huang, M. J. Collins, K. P. Chen, T. L. Hughes, and M. C. Rechtsman, Topological protection of photonic mid-gap defect modes, Nat. Photonics **12**, 408 (2018).

[18] C. W. Peterson, W. A. Benalcazar, T. L. Hughes, and G. Bahl, A quantized microwave quadrupole insulator with topologically protected corner states, Nature (London) **555**, 346 (2018).

[19] S. Imhof, C. Berger, F. Bayer, J. Brehm, L. W. Molenkamp, T. Kiessling, F. Schindler, C. H. Lee, M. Greiter, T. Neupert *et al.*, Topolectrical-circuit realization of topological corner modes, Nat. Phys. **14**, 925 (2018).

[20] M. Serra-Garcia, V. Peri, R. Süsstrunk, O. R. Bilal, T. Larsen, L. G. Villanueva, and S. D. Huber, Observation of a phononic quadrupole topological insulator, Nature (London) **555**, 342 (2018).

[21] G. Rosenberg and M. Franz, Witten effect in a crystalline topological insulator, Phys. Rev. B **82**, 035105 (2010).

[22] A. Leis, M. Schleenvoigt, V. Cherepanov, F. Lüpke, P. Schüffelgen, G. Mussler, D. Grützmacher, B. Voigtländer, and F. S. Tautz, Lifting the spin-momentum locking in ultra-thin topological insulator films, Adv. Quantum Technol. **4**, 2100083 (2021).

[23] Y. Zhang, K. He, C.-Z. Chang, C.-L. Song, L.-L. Wang, X. Chen, J.-F. Jia, Z. Fang, X. Dai, W.-Y. Shan, S.-Q. Shen, Q. Niu, X.-L. Qi, S.-C. Zhang, X.-C. Ma, and Q.-K. Xue, Crossover of the three-dimensional topological insulator Bi_2Se_3 to the two-dimensional limit, Nat. Phys. **6**, 584 (2010).

[24] Y. Sakamoto, T. Hirahara, H. Miyazaki, S.-I. Kimura, and S. Hasegawa, Spectroscopic evidence of a topological quantum

phase transition in ultrathin Bi_2Se_3 films, Phys. Rev. B **81**, 165432 (2010).
[25] A. K. Geim and I. V. Grigorieva, Van der Waals heterostructures, Nature (London) **499**, 419 (2013).
[26] C. Hu, K. N. Gordon, P. Liu, J. Liu, X. Zhou, P. Hao, D. Narayan, E. Emmanouilidou, H. Sun, Y. Liu, H. Brawer, A. P. Ramirez, L. Ding, H. Cao, Q. Liu, D. Dessau, and N. Ni, A van der Waals antiferromagnetic topological insulator with weak interlayer magnetic coupling, Nat. Commun. **11**, 97 (2020).
[27] S. K. Chong, K. B. Han, A. Nagaoka, R. Tsuchikawa, R. Liu, H. Liu, Z. V. Vardeny, D. A. Pesin, C. Lee, T. D. Sparks, and V. V. Deshpande, Topological insulator-based van der Waals heterostructures for effective control of massless and massive Dirac fermions, Nano Lett. **18**, 8047 (2018).
[28] L. Kou, S.-C. Wu, C. Felser, T. Frauenheim, C. Chen, and B. Yan, Robust 2D topological insulators in van der Waals heterostructures, ACS Nano **8**, 10448 (2014).
[29] S. Husain, R. Gupta, A. Kumar, P. Kumar, N. Behera, R. Brucas, S. Chaudhary, and P. Svedlindh, Emergence of spin–orbit torques in 2D transition metal dichalcogenides: A status update, Appl. Phys. Rev. **7**, 041312 (2020).
[30] D. Varsano, M. Palummo, E. Molinari, and M. Rontani, A monolayer transition-metal dichalcogenide as a topological excitonic insulator, Nat. Nanotechnol. **15**, 367 (2020).
[31] A. Kitaev, Periodic table for topological insulators and superconductors, AIP Conf. Proc. **1134**, 22 (2009).
[32] C.-K. Chiu, J. C. Y. Teo, A. P. Schnyder, and S. Ryu, Classification of topological quantum matter with symmetries, Rev. Mod. Phys. **88**, 035005 (2016).
[33] N. P. Armitage, E. J. Mele, and A. Vishwanath, Weyl and Dirac semimetals in three-dimensional solids, Rev. Mod. Phys. **90**, 015001 (2018).
[34] S. Lieu, M. McGinley, and N. R. Cooper, Tenfold way for quadratic Lindbladians, Phys. Rev. Lett. **124**, 040401 (2020).
[35] M. McGinley and N. R. Cooper, Topology of one-dimensional quantum systems out of equilibrium, Phys. Rev. Lett. **121**, 090401 (2018).
[36] A. M. Essin, J. E. Moore, and D. Vanderbilt, Magnetoelectric polarizability and axion electrodynamics in crystalline insulators, Phys. Rev. Lett. **102**, 146805 (2009).
[37] A. A. Burkov and L. Balents, Weyl semimetal in a topological insulator multilayer, Phys. Rev. Lett. **107**, 127205 (2011).
[38] J. E. Moore and L. Balents, Topological invariants of time-reversal-invariant band structures, Phys. Rev. B **75**, 121306(R) (2007).
[39] J. C. Y. Teo and C. L. Kane, Topological defects and gapless modes in insulators and superconductors, Phys. Rev. B **82**, 115120 (2010).
[40] F. Schindler, A. M. Cook, M. G. Vergniory, Z. Wang, S. S. P. Parkin, B. A. Bernevig, and T. Neupert, Higher-order topological insulators, Sci. Adv. **4**, eaat0346 (2018).
[41] A. Y. Kitaev, Unpaired Majorana fermions in quantum wires, Phys. Usp. **44**, 131 (2001).
[42] A. M. Cook, Topological skyrmion phases of matter, J. Phys.: Condens. Matter **35**, 184001 (2023).
[43] S.-W. Liu, L.-K. Shi, and A. M. Cook, Defect bulk-boundary correspondence of topological skyrmion phases of matter, Phys. Rev. B **107**, 235109 (2023).
[44] E. Prodan, Robustness of the spin-Chern number, Phys. Rev. B **80**, 125327 (2009).
[45] A. M. Cook, Quantum skyrmion Hall effect, (2023), arXiv:2305.18626 [cond-mat.str-el].
[46] N. N. Bogoljubov, On a new method in the theory of superconductivity, Il Nuovo Cimento **7**, 794 (1958).
[47] J. G. Valatin, Comments on the theory of superconductivity, Il Nuovo Cimento **7**, 843 (1958).
[48] See Supplemental Material at http://link.aps.org/supplemental/10.1103/PhysRevB.108.235102 for details on the spin topological invariant, observable-enriched entanglement spectra (OEES), and symmetry-protection ensuring gaplessness in OEES yields gaplessness in slab energy spectrum.
[49] D. Sticlet, F. Piéchon, J.-N. Fuchs, P. Kalugin, and P. Simon, Geometrical engineering of a two-band Chern insulator in two dimensions with arbitrary topological index, Phys. Rev. B **85**, 165456 (2012).
[50] I. Proskurin, M. Ogata, and Y. Suzumura, Longitudinal conductivity of a three-dimensional Dirac electron gas in magnetic field, J. Phys.: Conf. Ser. **603**, 012009 (2015).
[51] A. A. Abrikosov, Quantum magnetoresistance, Phys. Rev. B **58**, 2788 (1998).
[52] E. V. Gorbar, V. A. Miransky, and I. A. Shovkovy, Chiral anomaly, dimensional reduction, and magnetoresistivity of Weyl and Dirac semimetals, Phys. Rev. B **89**, 085126 (2014).
[53] U. Bajpai, M. J. H. Ku, and B. K. Nikolić, Robustness of quantized transport through edge states of finite length: Imaging current density in Floquet topological versus quantum spin and anomalous Hall insulators, Phys. Rev. Res. **2**, 033438 (2020).
[54] A. Alexandradinata, T. L. Hughes, and B. A. Bernevig, Trace index and spectral flow in the entanglement spectrum of topological insulators, Phys. Rev. B **84**, 195103 (2011).
[55] A. Alexandradinata, X. Dai, and B. A. Bernevig, Wilson-loop characterization of inversion-symmetric topological insulators, Phys. Rev. B **89**, 155114 (2014).